Theoretical Studies on the Reaction Mechanism of Platinum-Catalyzed Diboration of Allenes

Meiyan Wang,[†,‡] Lin Cheng,[†,‡] and Zhijian Wu*[,†]

State Key Laboratory of Rare Earth Resource Utilization, Changchun Institute of Applied Chemistry, Chinese Academy of Sciences, Changchun 130022, People's Republic of China, and Graduate School, Chinese Academy of Sciences, Beijing 100049, People's Republic of China

Received July 9, 2008

The reaction mechanism of Pt(0)-catalyzed diboration reaction of allenes is investigated by the density functional method B3LYP. The overall reaction mechanism is examined. The electronic mechanisms of the allene insertion into the Pt−B bond are discussed in terms of the electron donation, back-donation, and d−π interaction. During allene insertion into the Pt−B bond, the internal carbon atom of allene is preferred over the terminal one due to the stronger electron back-donation and stronger charge transfer in the former case than that in the latter one. By using the monosubstituted allenes (CN, Ph, Me, and NH_2), the influence of the substituents on the allene insertion into the Pt−B bond is analyzed. For CN, B−B bond addition to the terminal C═C bond of allene is favored over the internal one, while for Ph, Me, and NH_2, the internal one is preferred over the terminal one. This result can be explained by the influence of substituents on the charge transfer in the d−π interaction.

I. Introduction

Transition-metal complex catalyzed addition of element−element bonds to unsaturated organic molecules such as alkenes, alkynes, dienes, and allenes has attracted considerable interest due to their role in organic synthesis chemistry.[1−12] Dimetalation of allenes is especially interesting because the products, e.g., vinyl and/or allyl complexes, exhibit large potential applications for a wide variety of subsequent synthetic transformations. Diboration of allenes has been an efficient methodology to produce synthetically useful organoboron compounds with vinylboronate and allylboronate functional groups, which are effective in the asymmetric allylation of aldehydes to substituted homoallyl alcohols.[1−5,13]

Diboration of allenes was first studied using platinum catalysts by Miyaura and co-workers.[13] With monosubstituted allenes (in monosubstituted allene CH_2═C═CHR, the terminal and internal C═C bonds indicate C═CH_2 and C═CHR bonds, respectively), the B−B bond addition to the internal C═C bond was preferred over the terminal one, and the reaction mechanism was proposed to proceed by oxidative addition, allene insertion into the Pt−B bond to provide σ-vinyl or π-allyl platinum species, and finally reductive elimination. For various allenes, *Z*-stereoselectivity was obtained. In similar studies on the palladium-catalyzed diboration of allenes,[14−18] because the B−B bond oxidative addition to the palladium complex is an unfavored process from a theoretical aspect,[19] the palladium complexes failed to catalyze diboration of unsaturated carbon−carbon bonds. Therefore, the palladium-catalyzed diboration of allenes has to be conducted using the external Lewis basic ligands[14−17] or the external aryl or alkenyl iodide cocatalyst.[18] In the case of palladium catalyst with external Lewis basic ligands,[14−17] the regioselectivity with the two boryl groups connecting to the internal C═C bond of allenes is similar to that of the platinum catalysts,[13] while in the case of palladium catalyst with external aryl or alkenyl iodide cocatalyst, the opposite regioselectivity with the two boryl groups connecting to the terminal C═C bond of allenes was found. The difference of the regioselectivities originates from the different mechanisms of the reactions.[13,18]

Although the platinum catalysts were used to catalyze the diboration of allenes, the detailed reaction mechanism remains unclear. To understand the reaction mechanism, for nonsubstituted allene it is interesting to know to which carbon atom the boryl group prefers to connect, the terminal or the internal one in the insertion step? For monosubstituted allenes, in the insertion step, which carbon atom, the terminal, internal, or substituted one, is preferred? With the various monosubstituted allenes, what is the influence of substituents on the regioselectivity when the B−B bond adds to the terminal or internal C═C bond of the monosubstituted allenes? In fact, similar questions

* Corresponding author. Fax: +86-431-85698041. E-mail: zjwu@ciac.jl.cn.
† Changchun Institute of Applied Chemistry.
‡ Graduate School, Chinese Academy of Sciences.

(1) Burks, H. E.; Morken, J. P. *Chem. Commun.* **2007**, 4717.
(2) Beletskaya, I.; Moberg, C. *Chem. Rev.* **1999**, *99*, 3435.
(3) Beletskaya, I.; Moberg, C. *Chem. Rev.* **2006**, *106*, 2320.
(4) Suginome, M.; Ito, Y. *Chem. Rev.* **2000**, *100*, 3221.
(5) Ramı´rez, J.; Lillo, V.; Segarra, A. M.; Fernández, E. *C. R. Chim.* **2007**, *10*, 138.
(6) Marder, T. B.; Norman, N. C. *Top. Catal.* **1998**, *5*, 63.
(7) Ishiyama, T.; Miyaura, N. *Chem. Rec.* **2004**, *3*, 271.
(8) Clarke, M. L. *Polyhedron* **2001**, *20*, 151.
(9) Ishiyama, T.; Miyaura, N. *J. Organomet. Chem.* **2000**, *611*, 392.
(10) Suginome, M.; Ito, Y. *J. Organomet. Chem.* **2003**, *680*, 43.
(11) Torrent, M.; Sola, M.; Frenking, G. *Chem. Rev.* **2000**, *100*, 439.
(12) Huang, X.; Lin, Z. Y. In *Computational Modeling of Homogeneous Catalysis*; Maseras, F., Lledós, A., Eds.; Kluwer Academic Publishers: Amsterdam, 2002; pp 189−212.
(13) Ishiyama, T.; Kitano, T.; Miyaura, N. *Tetrahedron Lett.* **1998**, *39*, 2357.
(14) Pelz, N. F.; Woodward, A. R.; Burks, H. E.; Sieber, J. D.; Morken, J. P. *J. Am. Chem. Soc.* **2004**, *126*, 16328.
(15) Woodward, A. R.; Burks, H. E.; Chan, L. M.; Morken, J. P. *Org. Lett.* **2005**, *7*, 5505.
(16) Sieber, J. D.; Morken, J. P. *J. Am. Chem. Soc.* **2006**, *128*, 74.
(17) Burks, H. E.; Liu, S. B.; Morken, J. P. *J. Am. Chem. Soc.* **2007**, *129*, 8766.
(18) Yang, F. Y.; Cheng, C. H. *J. Am. Chem. Soc.* **2001**, *123*, 761.
(19) Cui, Q.; Musaev, D. G.; Morokuma, K. *Organometallics* **1998**, *17*, 742.

10.1021/om800645v CCC: $40.75
Publication on Web 11/11/2008

Scheme 1. Proposed Mechanism of the $Pt(PH_3)_2$-Catalyzed Allene Diboration Reaction

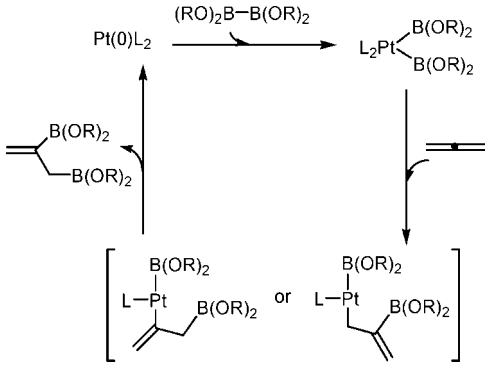

also exist in the palladium-catalyzed diboration of allene, although the palladium-catalyzed diboration of methylallene has been studied from experimental and theoretical aspects.[17] Recently, the palladium-catalyzed silaboration of methylallene has been studied theoretically.[20] It was found that the boryl group prefers to connect to the internal carbon atom of methylallene in the insertion step.

Based on theoretical studies on the Pd(0)-catalyzed diboration[17] and silaboration[20] of allenes, to understand the detailed mechanism of the Pt(0)-catalyzed allene diboration process, we have carried out theoretical calculations for the model reaction:

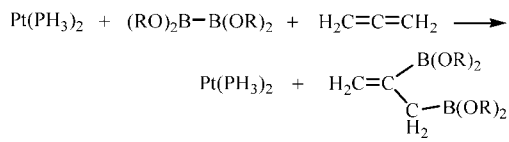

In the model reaction, the PPh_3 ligand in catalyst $Pt(PPh_3)_2$ was simplified to PH_3, while $(CH_2O)_2B-B(OCH_2)_2$ and allene $CH_2=C=CH_2$ were models for bis(pinacolato)diboron and substituted allenes in the experiment,[13] respectively. The simplification of PPh_3 to PH_3 was adopted by many previous studies and was shown to be reasonable for the study of the reaction mechanism.[19−23] In addition, $(CH_2O)_2B-B(OCH_2)_2$ was also a reasonable model for bis(pinacolato)diboron from the previous studies.[20,24−26] To study the regioselectivity of the B−B bond addition, monosubstituted allenes were used with the substituents cyano (CN), phenyl (Ph), methyl (Me), and amino (NH_2) groups.

II. Computational Methods

All calculations were performed using the Gaussian 03 suite of programs.[27] Geometries of the stationary points and transition states on the energy profiles were optimized by use of the B3LYP hybrid density functional theory.[28−30] For the basis set, double-ζ LANL2DZ was used for Pt, in which the effective core potentials (ECP) were used and mass-velocity and Darwin relativistic effects were incorporated.[31] For the remaining elements (i.e., C, H, P, B, O, and N atoms), the standard 6-311G(d) basis set was adopted. We denote the combination of the two basis sets (LANL2DZ for Pt, 6-311G(d) for the remaining atoms) as BSI. The optimization was carried out without imposing any symmetry constraints. Harmonic vibrational frequencies and thermal corrections to free energies were obtained at the same level of theory. Relative free energies were obtained by performing single-point calculations at the B3LYP level with LANL2DZ plus f-polarization[32] with an exponent of 0.993 for Pt and the 6-311+G(d,p) basis set for the remaining atoms (the combination of the two basis sets is named as BSII) using the above optimized geometries and by including thermal corrections to free energies at B3LYP/BSI, which includes entropy contributions by taking into account the vibrational, rotational, and translational motions of the species at 298.15 K. The stationary points and transition states on the energy profiles were confirmed by the normal-mode analysis. The intrinsic reaction coordinate (IRC) approach was used to confirm that the transition state indeed connects two relevant minima.[33,34] Natural population was made

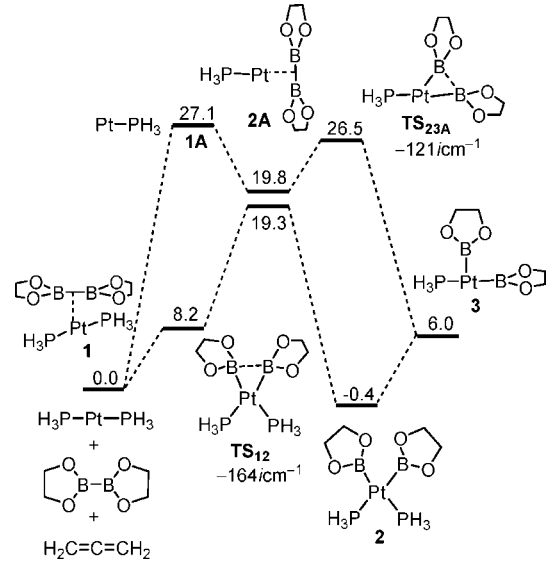

Figure 1. Calculated energy profiles for the oxidative addition of $[B(OR)_2]_2$ to $Pt(PH_3)_2$ [$Pt(PH_3)_2$ → **1** → **2**] and $Pt(PH_3)$ [$Pt(PH_3)_2$ → **1A** → **2A** → **3**]. The energy values (in kcal/mol) are the relative free energies.

(20) Abe, Y.; Kuramoto, K.; Ehara, M.; Nakatsuji, H.; Suginome, M.; Murakami, M.; Ito, Y. *Organometallics* **2008**, *27*, 1736.
(21) Cui, Q.; Musaev, D. G.; Morokuma, K. *Organometallics* **1997**, *16*, 1355.
(22) Cui, Q.; Musaev, D. G.; Morokuma, K. *Organometallics* **1998**, *17*, 1383.
(23) Zheng, W. X.; Ariafard, A.; Lin, Z. Y. *Organometallics* **2008**, *27*, 246.
(24) Zhao, H. T.; Lin, Z. Y.; Marder, T. B. *J. Am. Chem. Soc.* **2006**, *128*, 15637.
(25) Dang, L.; Zhao, H. T.; Lin, Z. Y.; Marder, T. B. *Organometallics* **2007**, *26*, 2824.
(26) Lam, K. C.; Lin, Z. Y.; Marder, T. B. *Organometallics* **2007**, *26*, 3149.
(27) Frisch, M. J.; Trucks, G. W.; Schlegel, H. B.; Scuseria, G. E.; Robb, M. A.; Cheeseman, J. R.; Montgomery, J. A., Jr.; Vreven, T.; Kudin, K. N.; Burant, J. C.; Millam, J. M.; Iyengar, S. S.; Tomasi, J.; Barone, V.; Mennucci, B.; Cossi, M.; Scalmani, G.; Rega, N.; Petersson, G. A.; Nakatsuji, H.; Hada, M.; Ehara, M.; Toyota, K.; Fukuda, R.; Hasegawa, J.; Ishida, M.; Nakajima, T.; Honda, Y.; Kitao, O.; Nakai, H.; Klene, M.; Li, X.; Knox, J. E.; Hratchian, H. P.; Cross, J. B.; Adamo, C.; Jaramillo, J.; Gomperts, R.; Stratmann, R. E.; Yazyev, O.; Austin, A. J.; Cammi, R.; Pomelli, C.; Ochterski, J. W.; Ayala, P. Y.; Morokuma, K.; Voth, G. A.; Salvador, P.; Dannenberg, J. J.; Zakrzewski, V. G.; Dapprich, S.; Daniels, A. D.; Strain, M. C.; Farkas, O.; Malick, D. K.; Rabuck, A. D.; Raghavachari, K.; Foresman, J. B.; Ortiz, J. V.; Cui, Q.; Baboul, A. G.; Clifford, J.; Cioslowski, J.; Stefanov, B. B.; Liu, G.; Liashenko, A.; Piskorz, P.; Komaromi, I.; Martin, R. L.; Fox, D. J.; Keith, T.; Al-Laham, M. A.; Peng, C. Y.; Nanayakkara, A.; Challacombe, M.; Gill, P. M. W.; Johnson, B.; Chen, W.; Wong, M. W.; Gonzalez, C.; Pople, J. A. *Gaussian 03*; Gaussian, Inc.: Pittsburgh, PA, 2003.
(28) Becke, A. D. *Phys. Rev. A* **1988**, *38*, 3098.
(29) Lee, C.; Yang, W.; Parr, R. G. *Phys. Rev. B* **1988**, *37*, 785.
(30) Becke, A. D. *J. Chem. Phys.* **1993**, *98*, 5648.
(31) Hay, P. J.; Wadt, W. R. *J. Chem. Phys.* **1985**, *82*, 299.
(32) Ehlers, A. W.; Böhme, M.; Dapprich, S.; Gobbi, A.; Höllwarth, A.; Jonas, V.; Köhler, K. F.; Stegmann, R.; Veldkamp, A.; Frenking, G. *Chem. Phys. Lett.* **1993**, *208*, 111.
(33) Fukui, K. *J. Phys. Chem.* **1970**, *74*, 4161.
(34) Fukui, K. *Acc. Chem. Res.* **1981**, *14*, 363.

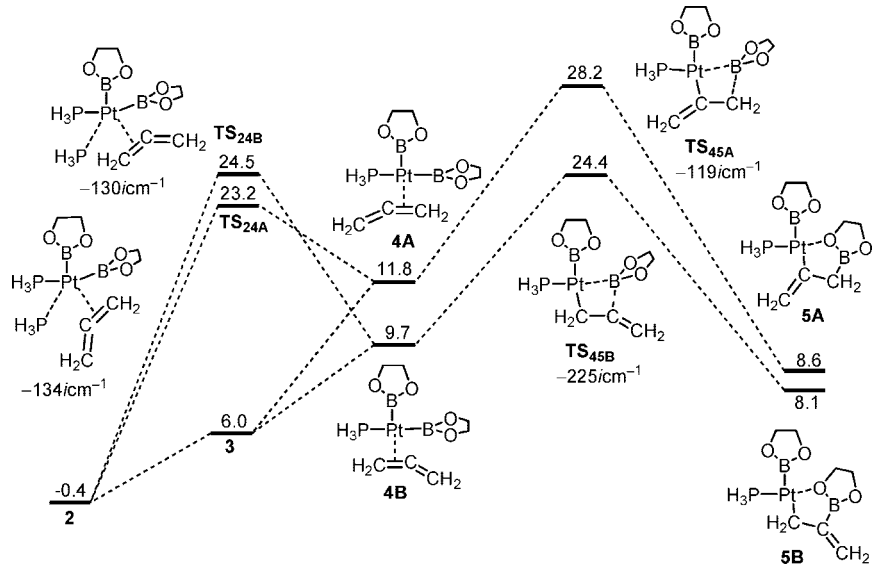

Figure 2. Calculated energy profiles for the allene coordination (**2** → **4A**; **2** → **4B**) and insertion into the Pt−B bond using the terminal carbon atom (1,2-insertion) (**4A** → $\mathbf{TS_{45A}}$ → **5A**) or the internal carbon atom (2,1-insertion) (**4B** → $\mathbf{TS_{45B}}$ → **5B**). The energy values (in kcal/mol) are the relative free energies. The values are relative to the initial reactants.

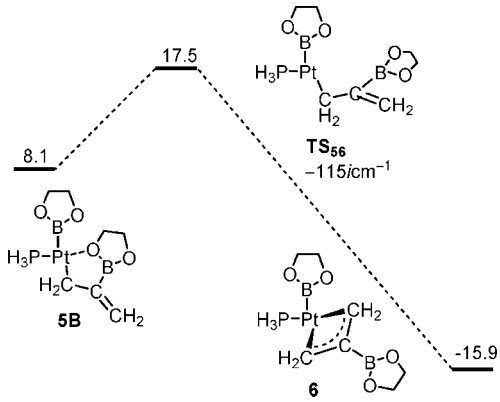

Figure 3. Calculated energy profile for the isomerization (**5B** → **6**). The energy values (in kcal/mol) are the relative free energies. The values are relative to the initial reactants.

by using the natural bond orbital (NBO) analysis.[35−37] The energies are all in kcal/mol.

III. Results and Discussion

The proposed mechanism of the Pt(0)-catalyzed allene diboration reaction based on the experiment[13] is presented in Scheme 1. In this mechanism, the B−B bond oxidatively adds to the Pt(0) complex and then the allene coordinates and inserts into the Pt−B bond using the terminal or internal carbon atom. Finally, the other boryl group migrates to the allene through a reductive elimination process. Between the allene insertion and reductive elimination, there are isomerization steps to facilitate the reductive elimination.

A. Oxidative Addition. Both the bisphosphine $Pt(PH_3)_2$ and monophosphine $Pt(PH_3)$ pathways are considered for the oxidative addition (Figure 1). In the bisphosphine pathway, the $(CH_2O)_2B-B(OCH_2)_2$ molecule initially coordinates to the Pt atom of $Pt(PH_3)_2$, forming the structure **1**. From **1**, the B−B bond in $(CH_2O)_2B-B(OCH_2)_2$ is activated through the transition state $\mathbf{TS_{12}}$, forming the oxidative addition product or intermediate bis(boryl)platinum(II) **2** with the two boryl groups in the *cis* position. The energy barrier of $\mathbf{TS_{12}}$ relative to the separated system or the initial reactants is calculated to be 19.3 kcal/mol. The dissociation of PH_3 from complex **2** forms complex **3**. In the monophosphine pathway, the dissociation of PH_3 costs an energy of 27.1 kcal/mol, forming $Pt(PH_3)$ **1A**. After that, the interaction of $(CH_2O)_2B-B(OCH_2)_2$ with **1A** gives the complex **2A**, from which the complex **3** is generated via transition state $\mathbf{TS_{23A}}$ with an energy barrier of 6.7 kcal/mol. Comparing the bisphosphine pathway $Pt(PH_3)_2$ → **1**→**2** → **3** with an energy barrier of 19.3 kcal/mol to the monophosphine pathway $Pt(PH_3)_2$ → **1A** → **2A** → **3** with an energy barrier of 27.1 kcal/mol, it is clear that the bisphosphine pathway is preferred over the monophosphine one.

B. Allene Coordination and Insertion. The next step is the coordination and insertion of allene to the bis(boryl)platinum(II) complex, producing the σ-vinyl or σ-allyl complex (Figure 2). For the allene coordination, there are two kinds of pathways. The first is the direct coordination of allene to complex **3**. The other is the phosphine dissociation from **2** and allene coordination to **2**, which take place simultaneously. In the first case, the coordination of allene to **3** generates the complexes **4A** and **4B**. In the other, the phosphine dissociation and allene coordination occur at the five-coordinate transition states $\mathbf{TS_{24A}}$ and $\mathbf{TS_{24B}}$ with energy barriers of 23.6 and 24.9 kcal/mol to form **4A** and **4B**, respectively. It is found that the pathways **2** → **3** → **4A** and **2** → **3** → **4B** are favored compared with **2** → $\mathbf{TS_{24A}}$ → **4A** and **2** → $\mathbf{TS_{24B}}$ → **4B**.

From complex **3**, the coordination of allene proceeds through two routes depending on the different orientations of the C=C bond of allene relative to the Pt−B bond. Allene insertion into the Pt−B bond using the terminal carbon atom takes place with a barrier of 16.4 kcal/mol at $\mathbf{TS_{45A}}$, giving the σ-vinyl complex **5A**, while allene insertion into the Pt−B bond using the internal carbon atom takes place with a barrier of 14.7 kcal/mol at $\mathbf{TS_{45B}}$, giving the σ-allyl complex **5B** (Figure 2). The transition state $\mathbf{TS_{45A}}$ is 3.8 kcal/mol higher than $\mathbf{TS_{45B}}$. The insertion product **5A** is 0.5 kcal/mol higher than **5B**. Therefore, the formation of

(35) Glendening, E. D.; Reed, A. E.; Carpenter, J. E.; Weinhold, F. NBO Version 3.1.
(36) Reed, A. E.; Curtiss, L. A.; Weinhold, F. *Chem. Rev.* **1988**, *88*, 849.
(37) Foster, J. P.; Weinhold, F. *J. Am. Chem. Soc.* **1980**, *102*, 7211.

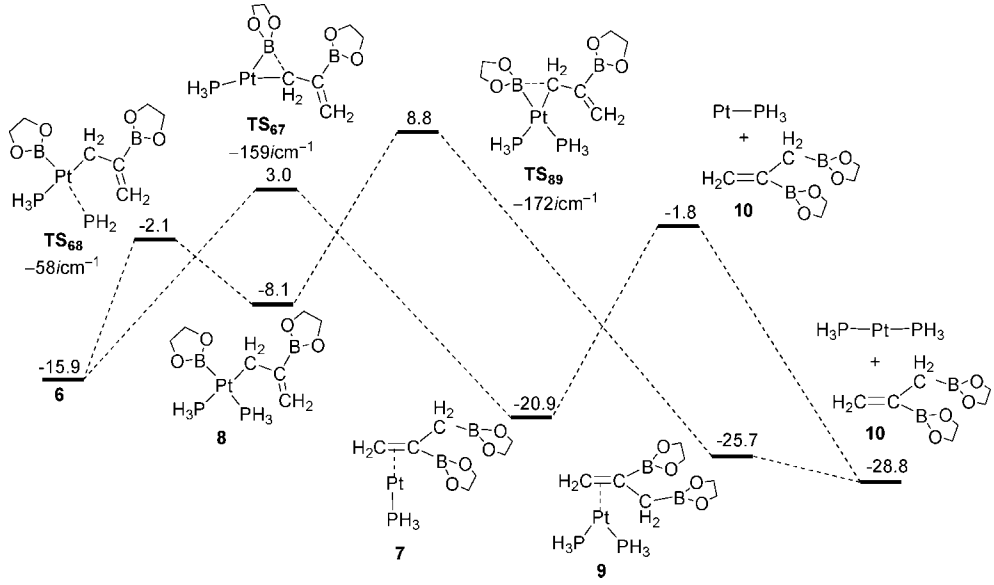

Figure 4. Calculated energy profiles for the reductive elimination of the product *Z*-CH_2=C[$B(OR)_2$]CH_2[$B(OR)_2$] **10** through the monophosphine (**6** → **7** → **10**) and bisphosphine (**6** → **8** → **9** → **10**) pathways. The energy values (in kcal/mol) are the relative free energies. The values are relative to the initial reactants.

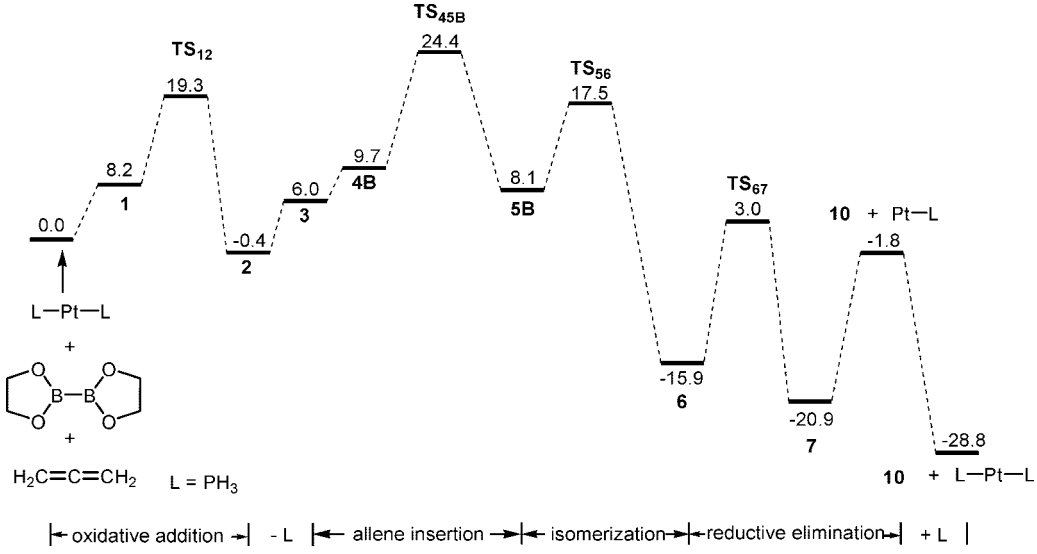

Figure 5. Calculated energy profile for the overall reaction of allene diboration catalyzed by $Pt(PH_3)_2$. The energy values are the relative free energies (in kcal/mol).

the σ-allyl complex **5B** is kinetically favored over that of σ-vinyl complex **5A**. In other words, the internal carbon atom of allene is preferred over the terminal one during allene insertion into the Pt−B bond. Thus, the reaction will continue along the pathway through **5B**.

C. Isomerization from σ-Allyl to π-Allyl Complex. The σ-allyl complex **5B** has an approximately planar structure with the boryl and allyl groups located in the *trans* orientation. A conversion from the σ-allyl complex to the π-allyl complex should occur to facilitate the reductive elimination, as in the silaboration of allenes.[20] The isomerization of σ-allyl complex **5B** takes place via the transition state $\mathbf{TS_{56}}$, generating the π-allyl complex **6** (Figure 3). Transition state $\mathbf{TS_{56}}$ is 6.9 kcal/mol lower than $\mathbf{TS_{45B}}$ (Figure 2), indicating that isomerization from the σ-allyl to the π-allyl complex is preferred over the β-elimination of boryl from **5B** to **4B**. It is also true for the silaboration of allenes that the insertion energy barrier is higher than the σ-allyl−π-allyl conversion barrier.[20] Interestingly, this σ-allyl−π-allyl conversion was not obtained for the palladium-catalyzed diboration of methylallene, because the π-allyl complex was formed directly in the methylallene insertion step.[17]

D. Reductive Elimination. From complex **6**, the reductive elimination takes place through two pathways, i.e., monophosphine and bisphosphine (Figure 4), as in the oxidative addition. In the monophosphine pathway, the reductive elimination takes place directly through the transition state $\mathbf{TS_{67}}$ with a barrier of 18.9 kcal/mol to form complex **7**. In the bisphosphine pathway, the recoordination of PH_3 takes place through the transition state $\mathbf{TS_{68}}$ with a barrier of 13.8 kcal/mol, generating complex **8**, from which the reductive elimination takes place via the transition state $\mathbf{TS_{89}}$ with a barrier of 16.9 kcal/mol to form complex **9**. The dissociation of $Pt(PH_3)$ and $Pt(PH_3)_2$ from the π-vinyl complexes **7** and **9** generates the final product *Z*-CH_2=C[$B(OCH_2)_2$]CH_2[$B(OCH_2)_2$] **10**. From Figure 4, the transition state $\mathbf{TS_{89}}$ is 5.8 kcal/mol higher than $\mathbf{TS_{67}}$. Thus, the reductive elimination prefers to proceed through the monophosphine pathway.

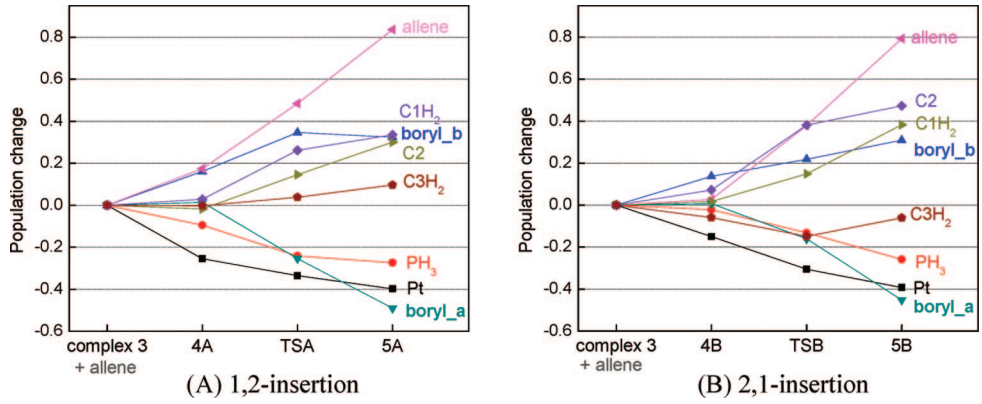

Figure 6. Population changes in the allene insertion into the Pt−B bond using the terminal carbon atom (1,2-insertion) and the internal carbon atom (2,1-insertion). A positive change means an increase in population, and vice versa.

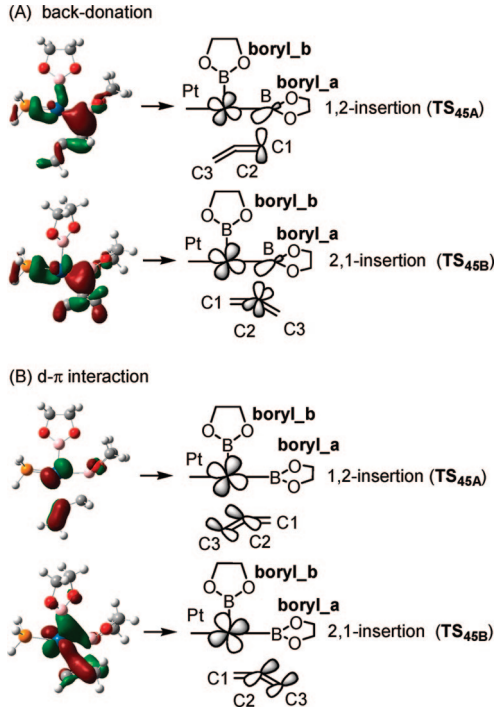

Figure 7. Molecular orbital diagram (left) and schematic diagram (right) of the orbital interactions (A) back-donation and (B) d−π interaction for the allene insertion into the Pt−B bond.

E. Reaction Mechanism. The overall reaction profile for the addition of the B−B bond to the C═C bond of allene catalyzed by $Pt(PH_3)_2$ is presented in Figure 5, and only the main reaction path is depicted. The present catalytic reaction proceeds exothermically to the product, and the rate-determining step is the insertion of allene into the Pt−B bond at the transition state **TS$_{45B}$** using the internal carbon atom. This is similar to the case of the palladium-catalyzed allene silaboration, in which the rate-determining step is also the allene insertion into the Pd−B bond using the internal carbon atom.[20] From Figure 5, the energy barrier of **TS$_{45B}$** is 24.4 and 24.8 kcal/mol compared with the initial reactants and the complex **2**, respectively. Complex **2**, i.e., the model of the bis(boryl)platinum(II) species in the experiment,[13] is involved in the overall reaction pathway, in agreement with the experimental observation[13] that the product was obtained from the stoichiometric reaction between allenes and bis(boryl)platinum(II) species.

For the allene insertion step, the two pathways through the transition states **TS$_{45A}$** and **TS$_{45B}$** are denoted as 1,2-insertion and 2,1-insertion for convenience of discussion. To investigate the electronic mechanism in 1,2- and 2,1-insertion processes, the natural orbital population changes in the two processes are shown in Figure 6. The boryl groups *trans* and *cis* to the phosphine ligand are marked as **boryl_a** and **boryl_b** as shown in Figure 7. It is seen that **boryl_a** connects to the terminal and internal carbon atom of allene for 1,2- and 2,1-insertion, respectively.

From the electronic mechanism, the electron donation and back-donation would be involved in the insertion step. From NBO calculations, the charge of the allene group is −0.48 and −0.38 for 1,2- (**TS$_{45A}$**) and 2,1-insertion (**TS$_{45B}$**), respectively. This shows that the allene group gains electrons in both 1,2- and 2,1-insertion. Therefore, the electron back-donation should be much stronger than the electron donation for both 1,2- and 2,1-insertion, which is also observed for CO_2 (ref 24) or alkene[25] insertion into the Cu−B bond. Thus, electron back-donation is examined for both 1,2- and 2,1-insertion.

In Figure 7A, it is seen that electron back-donation is from the Pt−B σ-bonding orbital to the allene unhybridized p orbital. In allene, the internal carbon atom C2 is sp hybridized, while the terminal carbon atom C1 (and C3) is sp^2 hybridized. Thus, the internal carbon atom C2 has two unhybridized p orbitals, which might interact more strongly than the terminal carbon atom C1, which has only one unhybridized p orbital. In 1,2-insertion, it is the terminal carbon atom C1 with one unhybridized p orbital that interacts with the Pt−B σ-bonding orbital, while it is the internal carbon atom C2 with two unhybridized p orbitals in 2,1-insertion. Therefore, the electron back-donation could be stronger for 2,1-insertion than 1,2-insertion. This is also confirmed by the population change, in which the internal carbon atom C2 in **TS$_{45B}$** has a larger population than the terminal group $C1H_2$ in **TS$_{45A}$** (Figure 6).

On the other hand, by analyzing the interaction between the occupied Pt d orbital and the π-bonding orbital of allene, the d−π interaction is observed (Figure 7B). Since the overlap between the Pt d orbital and the allene π-bonding orbital in the d−π interaction delocalizes the electron distribution, the d−π interaction will stabilize the transition state **TS$_{45A}$** and **TS$_{45B}$**.

For both 1,2- and 2,1-insertion, the d−π interaction is through the internal carbon atom C2 and terminal group $C3H_2$ of allene. Thus, C2 is involved not only in the back-donation of **TS$_{45B}$** as mentioned earlier but also in the d−π interaction of **TS$_{45A}$** and **TS$_{45B}$**. At **TS$_{45A}$**, the electron population change of $C3H_2$ is quite small (Figure 6), suggesting that the charge transfer between the Pt d orbital and the allene π-bonding orbital in the d−π interaction would be small. Therefore, in the 1,2-insertion, the

Scheme 2. Possible Reaction Scheme for the Insertion Step with Monosubstituted Allene $H_2C{=}C{=}CHR$ (R = CN, Ph, Me, and NH_2)[a]

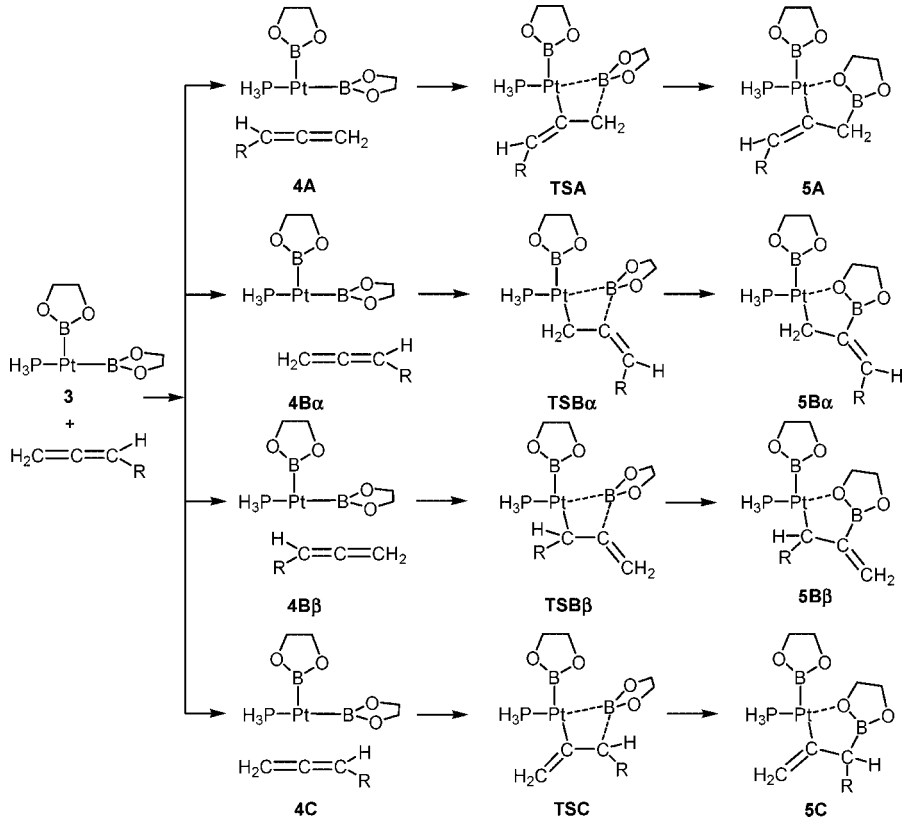

[a] A, B, and C represent the monosubstituted allene insertion into the Pt−B bond using the terminal, internal, and substituted carbon atoms, respectively; α and β indicate the substituent on the boryl and phosphine side, respectively.

influence of the d−π interaction on the stability of transition state **TS_{45A}** could be minor. At **TS_{45B}**, however, the $C3H_2$ group loses relatively more electrons (Figure 6). This indicates that the charge transfer of the d−π interaction is from the allene π-bonding orbital to the Pt d orbital. Thus, the charge transfer of the d−π interaction has a large influence on the stability of **TS_{45B}**. Because of the stronger electron back-donation and stronger charge transfer of the d−π interaction at **TS_{45B}** than those at **TS_{45A}**, the transition state **TS_{45B}** becomes more stable than **TS_{45A}**; that is, 2,1-insertion is preferred to 1,2-insertion. In addition, since all the groups in allene ($C1H_2$, C2, and $C3H_2$) gain electrons at **TS_{45A}**, while $C3H_2$ loses electrons at **TS_{45B}** (Figure 6), this might explain the fact that the charge of the allene group in **TS_{45B}** (−0.38) is less negative than **TS_{45A}** (−0.48).

From the overall reaction profile (Figure 5), although the allene insertion into the Pt−B bond is the rate-determining step for allene diboration, the isomerization from the σ-allyl to the π-allyl complex determines B−B bond addition to the terminal or internal C═C bond for monosubstituted allenes. Therefore, it would be interesting to examine the insertion and isomerization steps for the monosubstituted allenes.

F. Regioselectivities for the Monosubstituted Allene Diboration. Scheme 2 shows the possible insertion reactions for the monosubstituted allenes with substituents CN, Ph, Me, and NH_2. The complexes **4A**, **4Bα**, **4B*β***, and **4C** give the transition states **TSA**, **TSBα**, **TSB*β***, and **TSC**, which lead to the four corresponding insertion products **5A**, **5Bα**, **5B*β***, and **5C**, respectively, where A, B, and C represent the monosubstituted allene insertion into the Pt−B bond using the terminal, internal, and substituted carbon atoms, respectively; α and β indicate the substituent on the boryl and phosphine side, respectively.

From Figure 8, the energy of transition states increases in the order **TSBx** (x = α, β), **TSA**, and **TSC** for CN, Ph, and Me, while **TSA** is more stable than **TSB*β*** for NH_2. For **TSBx** (x = α, β), the energy of **TSBα** is lower than **TSB*β*** for the monosubstituted allenes except for CN, in which the opposite case is obtained. Since the transition states **TSBx** (x = α, β) are lower in energy than **TSA** and **TSC**, the next isomerization step from the insertion products **5Bx** (x = α, β) is examined, which is related to the B−B bond addition to the internal or terminal C═C bond of monosubstituted allenes. Scheme 3 shows the possible isomerization process for the monosubstituted allenes with substituents CN, Ph, Me, and NH_2. The B−B bond addition to the internal and terminal C═C bond of monosubstituted allenes would give the corresponding final products **10α** and **10*β***. From Figure 8, it is evident that the insertion step determines the B−B bond addition to the terminal C═C bond or the internal one, because the energy of isomerization transition states **TS_{56x}** (x = α, β) is lower than that of the corresponding insertion transition states **TSBx** (x = α, β) for CN, Ph, Me, and NH_2.

Cyanoallene. It is noted that for R = CN (Figure 8A) **TSBα** lies 3.2 kcal/mol higher than **TSB*β***, showing that the insertion into the terminal C═C bond is favored over the internal one. From the orbital interactions (Figure 7), since the electron back-donation occurs on the internal carbon atom at both **TSBα** and **TSB*β***, the influence of the electron back-donation is minor for **TSBα** compared with **TSB*β***. Thus, for comparison, the d−-π interaction is examined for both **TSBα** and **TSB*β***. CN is an

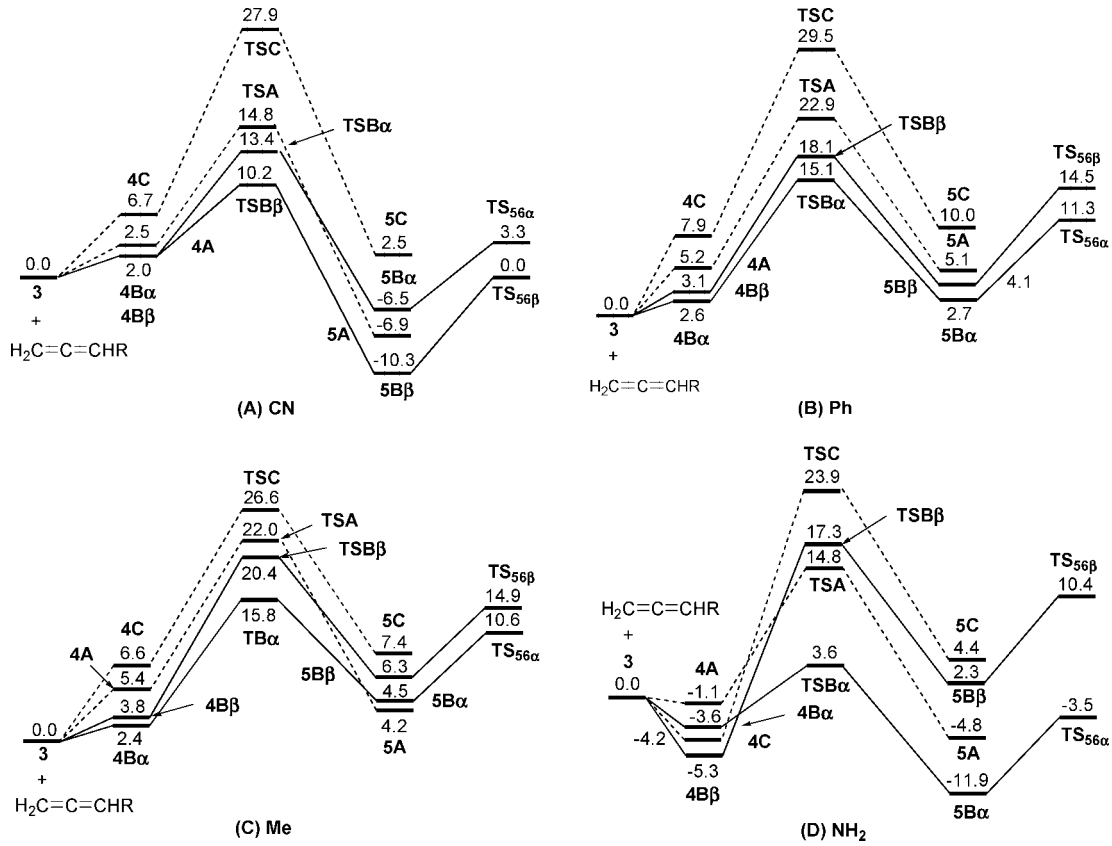

Figure 8. Calculated energy profiles for the insertion and isomerization steps. The substituents R are (A) CN, (B) Ph, (C) Me, and (D) NH_2. The energy values (in kcal/mol) are the relative free energies. The values are relative to complex **3** and the corresponding monosubstituted allenes.

Scheme 3. Possible Reaction Scheme for the Isomerization Step with Momosubstituted Allenes $H_2C{=}C{=}CHR$ (R = CN, Ph, Me, and NH_2)[a]

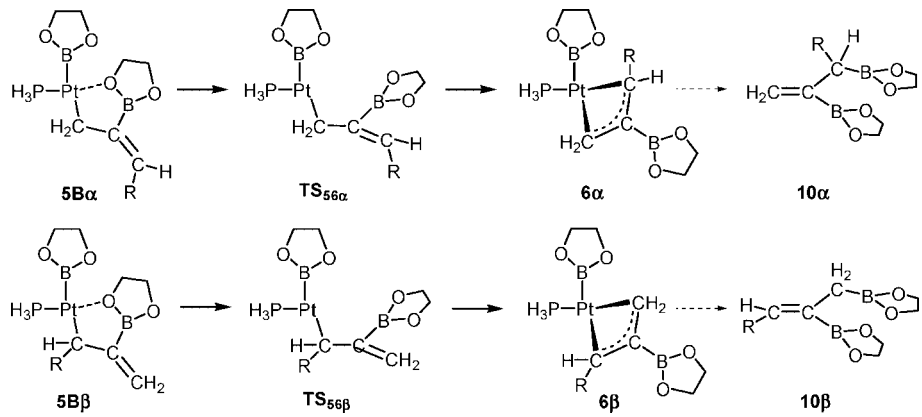

[a] α and β represent the two $B(OR)_2$ groups added to the internal and terminal C═C bond, respectively.

electron-withdrawing group and can form π conjugation with the surrounding p orbitals. At **TSBα**, the substituent CN is involved in the d−π interaction. Therefore, the π conjugation of CN could participate in the d−π interaction and withdraw electrons through d−π interaction. This would weaken the charge transfer in the d−π interaction at **TSBα**. However, the π conjugation of CN does not exist at **TSBβ** because CN is not involved in the d−π interaction. Thus, B−B bond addition to the terminal C═C bond (**TSBβ**) is preferred over the internal one (**TSBα**) due to the involvement of the electron-withdrawing conjugation group CN.

Phenylallene. **TSBα** lies 3.0 kcal/mol lower than **TSBβ**, indicating that B−B bond addition to the internal C═C bond of phenylallene is favored over that to the terminal one (Figure 8B). This is opposite the case in cyanoallene. Similar to the case of cyanoallene, the electron back-donation has minor influence for **TSBα** compared with **TSBβ**. At **TSBα**, the π conjugation of the phenyl group is related to the d−π interaction of the cyano group. The difference between phenyl and cyano groups is that phenyl is electron-donating, while cyano is electron-withdrawing. The electron-donating phenyl group would enhance the d−π interaction. Thus, B−B bond addition to the internal C═C bond (**TSBα**) is preferred over the terminal one (**TSBβ**).

Methylallene. The B−B bond addition to the internal C═C bond of methylallene is favored over the terminal one due to

the fact that **TSBα** lies 4.6 kcal/mol lower than **TSBβ** (Figure 8C), which is similar to the case of phenylallene. At transition state **TSBα**, the d−π interaction is strengthened, because the methyl group is electron-donating and the electron transfer in the d−π interaction is from the π bonding of methylallene to the d orbital of the Pt atom. In other words, the electron-donating group is helpful to decrease the energy of transition state **TSBα** during B−B bond addition to the internal C═C bond.

Aminoallene. For R = NH_2 (Figure 8D), the complexes **4A**, **4Bα**, **4Bβ**, and **4C** have the lowest relative energy compared with substituents CN, Ph, and Me due to the increase of the electron density on aminoallene induced by the more electron-donating substituent NH_2. **TSBα** lies 13.7 kcal/mol lower than **TSBβ**, indicating that the internal C═C bond is favored over the terminal one, as in the case of methylallene.

In the monosubstituted allene insertion step, the boryl group prefers to connect to the internal carbon atom over the terminal and the substituted one for CN, Ph, Me, and NH_2. The reason is that the d−π interaction between the $Pt[B(OCH_2)_2]_2(PH_3)$ complex and monosubstituted allene group exists for the boryl connection to the internal carbon atom process, and it is significant for electron transfer from the monosubstituted allene group to the Pt complex. For the regioselectivity, the internal C═C bond is favored over the terminal one for Ph, Me, and NH_2, while it is opposite for CN. This indicates that the B−B bond addition to the internal C═C bond of monosubstituted allenes is preferred for electron-donating groups and to the terminal one for electron-withdrawing groups, due to the influence of the substituent on the d−π interaction.

IV. Conclusions

The Pt(0)-catalyzed allene diboration reaction has been studied by using the hybrid density functional method B3LYP. The overall reaction pathways are examined. The favorable reaction pathway proceeds via the following steps: (a) oxidative addition of B−B to $Pt(PH_3)_2$, (b) dissociation of PH_3 from $Pt[B(OR)_2]_2(PH_3)_2$ to form complex $Pt[B(OR)_2]_2(PH_3)$, (c) allene coordination and insertion into the Pt−B bond, (d) isomerization from the σ-allyl to π-allyl complex, and (e) reductive elimination to give the final product Z-CH_2═$C[B(OR)_2]CH_2[B(OR)_2]$. It is found that the internal carbon atom is favored over the terminal one during the allene insertion into the Pt−B bond and can be explained by the stronger electron back-donation and stronger charge transfer in the d−π interaction in the former case than that in the latter case. For monosubstituted allenes (CN, Ph, Me, and NH_2), B−B bond addition to the terminal C═C bond is preferred over the internal one for CN, while the internal one is favored over the terminal one for Ph, Me, and NH_2, which can be explained from the influence of substituents on the charge transfer in the d−π interaction.

Acknowledgment. The authors thank the National Natural Science Foundation of China for financial support (Grant 20773117).

Supporting Information Available: Cartesian coordinates of the allenes diboration catalyzed by $Pt(PH_3)_2$ from the optimized geometries. This material is available free of charge via the Internet at http://pubs.acs.org.

OM800645V